



AIAA 2003-4085

**Evaluation of a Second-Order Accurate
Navier-Stokes Code for
Detached Eddy Simulation Past a Circular
Cylinder**

Veer N. Vatsa

and

Bart A. Singer

NASA Langley Research Center

Hampton, VA 23681

**21st AIAA Applied Aerodynamics
Conference**

June 23-26, 2003

Orlando, Florida

For permission to copy or to republish, contact the copyright owner named on the first page.

For AIAA-held copyright, write to AIAA Permissions Department,
1801 Alexander Bell Drive, Suite 500, Reston, VA, 20191-4344.

Evaluation of a Second-Order Accurate Navier-Stokes Code for Detached Eddy Simulation Past a Circular Cylinder

Veer N. Vatsa* and Bart A. Singer †
 NASA Langley Research Center
 Hampton, VA

Abstract

We evaluate the applicability of a production computational fluid dynamics code for conducting detached eddy simulation for unsteady flows. A second-order accurate Navier-Stokes code developed at NASA Langley Research Center, known as TLNS3D, is used for these simulations. We focus our attention on high Reynolds number flow ($Re = 5 \times 10^4 - 1.4 \times 10^5$) past a circular cylinder to simulate flows with large-scale separations. We consider two types of flow situations: one in which the flow at the separation point is laminar, and the other in which the flow is already turbulent when it detaches from the surface of the cylinder. Solutions are presented for two- and three-dimensional calculations using both the unsteady Reynolds-averaged Navier-Stokes paradigm and the detached eddy simulation treatment. All calculations use the standard Spalart-Allmaras turbulence model as the base model.

Introduction

Despite the phenomenal growth of computational fluid dynamics (CFD) in last three decades, significant barriers still exist for routine computations of high Reynolds number, highly separated and unsteady flows. Even with the continuous and steady growth in computational power realized during this period, the simulation of three-dimensional (3-D) unsteady flows is still a computationally intensive task. Most of the turbulence models in use today were developed with statistically steady-state assumptions and databases from the very outset, and hence are of uncertain accuracy for simulating unsteady (non stationary) flows.

Spalart has discussed the various levels of modeling required for simulating unsteady separated flows.¹⁻³ He considers the temporal and spatial resolution of large eddies (vortices) to be of fundamental importance for massively separated flows. Full 3-D simulations are required for such large separated flows, even for nominally two-dimensional (2-D) geometries.⁴ Large eddy simulation (LES), in which the large eddies are resolved and smaller

eddies in the near wall region are modeled, is considered a reasonable choice for simulating such flow problems. However, the computational costs for LES simulations for aircraft configurations based on Spalart's estimates⁵ make such an approach impractical for routine computations.

As an alternative, a family of turbulence treatments, which can be classified as hybrids of LES and Reynolds averaged Navier-Stokes (RANS) simulations, have been proposed in recent years for predicting time-dependent separated flows. The most notable in this family are: detached eddy simulation (DES) of Spalart,³ hybrid RANS-LES model of Arunajatesan and Sinha,⁶ limited numerical scales (LNS) model of Batten et al.,⁷ and flow simulation methodology (FSM) of von Terzi and Fasel.⁸ The basic idea used in the hybrid models was proposed by Speziale.⁹ It involves the coupling of a standard turbulence model in regions where the turbulence is dominated by small scales, with an LES-type treatment in the regions where the large scale unsteady turbulent structures are resolvable. In the regions of resolvable large-scale structures, the large eddies can be simulated by solving the unsteady RANS (URANS) equations with a modified model to provide reduced levels of dissipation. Based on the number of publications that have appeared in the literature in the last few years,^{4,10-14} the DES treatment of Spalart³ appears to be the most popular among the various hybrid models. One of the reasons for its popularity is the ease with which it can be implemented into a production CFD code. The primary goal of this paper is to assess how well the DES treatment performs in such a code.

Approach

A widely used Navier-Stokes flow code, known as TLNS3D, is applied to compute flow past a circular cylinder at high Reynolds number. This code, which is nominally second-order accurate in space and time, has been tested extensively by NASA and industry researchers for solving subsonic, transonic, and supersonic flows over aerodynamic configurations of practical interest. The one-equation Spalart-Allmaras (S-A) model,¹⁵ and Menter's two-equation model¹⁶ are two of the most popular turbulence models available in TLNS3D. The DES treatment³ in conjunction with the S-A turbulence

*Senior Member, AIAA

†Senior Member, AIAA

This material is declared a work of the U.S. Government and is not subject to copyright protection in the United States.

model is also available in the TLNS3D code.

A cell-centered finite volume scheme supplemented with matrix dissipation is used for spatial discretization in TLNS3D. A multi-stage Runge-Kutta time-stepping scheme patterned after the Jameson-Schmidt-Turkel scheme,¹⁷ is used for advancing the solution in pseudo-time to obtain steady-state solutions. Convergence acceleration is obtained through the use of local time stepping, implicit residual smoothing and a multi-grid technique. For time-accurate solutions, the dual time-stepping scheme proposed by Jameson,¹⁸ and further developed by Melson and Sanetrik¹⁹ is employed. The TLNS3D code has the option of evaluating the time derivatives either by using backward differencing formulas (for up to third-order accuracy) or by using the implicit Runge-Kutta scheme²⁰ to obtain higher order (up to fifth-order) temporal accuracy.

For the present paper, we used the finest overset sectional grid (210x135) from the work of Travin et al.,²¹ as an initial grid. We created a multi block, C_0 continuous grid that is comparable to the initial grid in the downstream wake regions and merges smoothly with the initial grid in the upstream region. The resulting grid has 32,256 cells in the 2-D plane describing the circular cylinder immersed in free air. This grid, shown in Fig. 1, is referred to as the baseline grid in this paper.

Second-order backward difference temporal discretization is used in this study due to its superior robustness and stability properties. The physical time step selected for the solutions presented in this paper was based on a series of 2-D runs made with successively smaller values of time step, until phase and amplitude errors in integrated forces became negligible. The baseline value of time step arrived in this manner corresponded to having approximately 100 points in each vortex shedding cycle.

Results

The results are presented under two main categories: turbulent separated (TS) cases and laminar separated (LS) cases. For the TS cases, the code is run in the standard production mode, with free-stream turbulence levels selected to be high enough to cause natural transition to turbulent flows before the flow separates at the surface of the cylinder. Because the transition point is not known a priori for the LS cases, we employ the tripless approach of Shur et al.²² In this approach, an initial solution is obtained by specifying a small value of eddy viscosity at the inflow, which generates eddy viscosity in the entire field. In subsequent runs, the flow field from this case is used as a starting solution, and the value of eddy viscosity is set to zero at the inflow. Thus the initial values of eddy viscosity are convected out of the computational domain and the upstream part of the boundary

layer develops with zero eddy viscosity, or as a laminar flow. However, the recirculation zone has non-zero eddy viscosity, which propagates upstream to the point of detachment. Beyond the point of detachment, the eddy viscosity diffuses into the separating shear layer. In this approach, the location and extent of transition does not need to be specified, and hence it is known as tripless transition. A free stream Mach number of 0.2 is used for all the computations presented here.

Turbulent Separated (TS) Case

The TS case simulates the experimental flow conditions where the boundary layer is tripped well ahead of separation. We achieve this objective numerically by choosing free stream turbulence levels that are high enough to cause natural transition. Travin et al.²¹ showed that this test case is relatively insensitive to the Reynolds number. They performed most of their computations at a Reynolds number of 1.4×10^5 , although the experimental data used for the comparisons are at much higher Reynolds number. We performed URANS computations with TLNS3D at the Reynolds number of 1.4×10^5 to match the conditions used by Travin et al.²¹ The time-averaged values of pressure coefficients (C_p) at the cylinder resulting from the 2-D computations on the baseline grid are compared with the experimental data of Roshko²³ and van Nunen²⁴ in Fig. 2, where Φ denotes the circumferential angle for the cylinder. The computational results on a finer grid (FG) with twice as many points in both directions, also shown in this figure, indicate very little effect of grid refinement giving us confidence in the numerical accuracy of the present solutions. The 2-D URANS solutions of Travin et al.²¹ are compared with TLNS3D solutions in Fig. 3. Based on these results, it is concluded that the current 2-D URANS (time-averaged) solutions are essentially grid converged and compare reasonably well with the experimental data of van Nunen²⁴ and with the higher order accurate solutions of Travin et al.²¹

The 3-D DES results from the work of Travin et al.²¹ are also plotted in Fig. 3, and only small differences are observed between 2-D URANS and 3-D DES results. The similarity between these time-mean solutions should not be understood to extend to the time-dependent flow features. The similarity of the mean flow results for the TS cases is likely due to the fact that this flow has a narrow wake, which is relatively stable. To get a quantitative estimate on the size of the wake, the time-averaged total pressure contours from TLNS3D solutions are plotted in Fig. 4. The low pressure region seen in this figure delineates the wake region behind the cylinder. The maximum value chosen for this plot is 0.98 to emphasize the wake region. This figure clearly shows a relatively small and narrow wake for the TS calculations. Such

confined wakes are accompanied by weak shedding and mild three-dimensionality. For this reason, we did not pursue 3-D simulations for TS cases; instead we focus our attention on the more sensitive LS cases in rest of this paper.

Laminar Separated (LS) Case

The LS cases were run with the tripless transition approach (described earlier in the paper) in order to ensure that the boundary layer flow approaching the separation point on the cylinder is laminar. The computations reported here were performed at a Reynolds number of 5×10^4 to match the conditions of Travin et al.²¹ The 2-D URANS solutions obtained with the TLNS3D code are shown in Fig. 5 on the baseline grid and on a finer grid (FG) consisting of twice the number of grid points in each direction compared to the baseline grid. The experimental data of Cantwell and Coles²⁵ are also shown in this figure, along with the 2-D URANS results of Travin et al.²¹ This figure shows that the effect of grid refinement is minimal on the surface pressure distributions. We also observe that the agreement between the present results and those of Travin et al.²¹ is quite good up to about $\Phi = 100^\circ$, after which the quantitative agreement deteriorates. Differences in the implementation of initial and far-field boundary conditions, and turbulence modeling in the two computational approaches could contribute to the differences in computational results observed in this figure. More importantly, both of these calculations show similar inaccurate pressure levels in the base region ($\Phi > 100^\circ$) of the cylinder.

The next set of solutions were obtained by using the 2-D DES approach for this case. The pressure distribution from TLNS3D computations compares favorably with the 2-D DES results of Travin et al.,²¹ as seen in Fig. 6. However, the agreement between the 2-D DES results and the experimental data in the base region of the cylinder is poor. Spalart³ suspects that non-physical solutions might result from using 2-D DES and he advises against it. The main reason for this exercise was to demonstrate that TLNS3D reproduces the flow features observed by the higher order schemes for different turbulence treatments currently being practiced for simulating highly separated flows.

We now focus attention on the 3-D simulations. Having established the adequacy of the baseline grid for 2-D simulations, we constructed the 3-D grid by stacking 41 planes of the baseline grid in the spanwise direction. Such a spanwise grid is comparable to the grids used in the work of Travin et al.²¹ Due to the limited computing resources available, the 3-D simulations were spread over multiple runs. Once the flow displayed the expected quasi-periodic behavior, running averages were computed and stored during the subsequent runs. The

computations were continued until the time-averaged surface pressure distributions converged to plotting accuracy.

The time-averaged surface pressure distributions from the 3-D URANS computations are compared with the 2-D URANS and the experimental data in Fig. 7. Compared with the 2-D URANS results, the 3-D URANS results are much closer to the experimental data. The primary reason for this is the spanwise relief of the wake vortex stretching afforded in the 3-D simulations. However, the eddy viscosity level, and hence the dissipation is still too high in free shear layer regions. The 3-D DES simulations were then performed to address this shortcoming, and the resulting solutions are found to be much closer to the experimental data. The 3-D DES solutions on two grids, consisting of 150x109x42 and 210x135x57 points (designated as MG and FG, respectively) from Travin et al.²¹ are also shown in this figure. Keeping in mind the various sources of numerical differences in the two schemes, and that grid convergence is not straight forward for DES solutions,³ the agreement between these independently obtained 3-D DES solutions is considered quite good.

The time-averaged eddy-viscosity fields resulting from the standard URANS and the DES computations are shown in Figs. 8 and 9. The contour plots are scaled with the maximum value of eddy viscosity from the DES calculations. The region behind the cylinder in Fig. 9 displays a zone devoid of any contour lines, which corresponds to the region in which eddy viscosities exceed this maximum. In fact, the URANS calculations indicate a maximum of about 1000 in this zone, which is over four times the maximum from the DES calculations. This is the zone where the DES treatment is effective. The DES simulation produces eddy viscosities in this zone that are appropriate for a large-eddy simulation, rather than the more heavily damped viscosities typical of URANS calculations. The reduced viscosities in the wake region allows the DES to more accurately simulate the large-scale fluctuating flow in that region.

Before concluding this section, we would like to comment on the numerical accuracy of the present computational results. Although we recognize that the temporal and spatial accuracies may be coupled for unsteady calculations, we examined them separately for convenience. For temporal accuracy, we repeated the 3-D simulations with half the time step and observed less than 0.5 % effect on the average lift and drag coefficients. For spatial accuracy, we already showed minimal effect of grid doubling on the 2-D simulations from the baseline grid solutions. In addition, we incorporated a fourth-order accurate discretization of convective terms into the TLNS3D code, replacing the standard second-order discretization. Such an approach mimics the higher order

schemes, which employ higher order construction for the convective terms, but treat the diffusion terms and turbulence models with second-order discretization. The solutions obtained with this higher order treatment are compared with the second-order solutions and the experimental data in Fig. 10. Based on these comparisons, it is apparent that the truncation errors due to the convective operators are small for these 3-D DES simulations, giving us further confidence in the ability of nominally second-order TLNS3D code to accurately simulate unsteady flows with large embedded separated regions.

Time-Dependent Behavior

Time histories for the 3-D URANS and 3-D DES integrated forces for the LS case are shown in Figs. 11 and 12. The lift (Cl) and drag (Cd) coefficients for the 3-D URANS simulations display nearly periodic and regular oscillations with small variations in peak values for these forces. The 3-D DES solutions on the other hand display large and random variations in the body forces, indicative of strong modulations of the vortex shedding. These observations are very similar to the ones reported by Travin et al.,²¹ and are consistent with physical expectations for highly separated flows. The time histories with higher order (fourth-order) discretizations of convective terms are shown in Fig. 13. The reason for different time locations for lows and highs in the modulations is due to a shift in the time scale introduced by different starting points for these simulations, which creates a shift in the virtual origin of the time axis in these figures. Overall, the effect of fourth-order convective discretization (compared with standard second-order discretization) on the integrated forces is considered minimal.

The instantaneous vorticity magnitude contours in the mid-plane of the cylinder for the second-order 3-D DES simulations at time instances in proximity of low- and high-lift oscillations are shown in Figs. 14 and 15, respectively. The vorticity patterns displayed in these figures indicate entirely different structures for these instances in time. The overall structural details are comparable to the results of Travin et al.²¹ However, somewhat finer structures were observed in the results of Travin et al.,²¹ possibly due to use of a higher order scheme. Fig. 16 shows a snapshot of the vorticity contours near high-lift oscillations (but not at the same lift) based on the fourth-order convective discretizations in 3-D DES TLNS3D simulations. As expected, finer vortical structures are captured by the higher order scheme. However, recall that despite a noticeable effect of the spatial order of the scheme on instantaneous flow quantities and time histories, the resulting time averaged pressures on the cylinder surface were found to be relatively insensitive to such changes.

Concluding Remarks and Future Directions

A nominally second-order accurate flow code, known as TLNS3D, has been evaluated for computing highly separated, unsteady flows past a circular cylinder. For the turbulent separated cases, in which the oncoming boundary layer is turbulent ahead of the separation point, the surface pressures are reasonably well predicted by running the code in 2-D mode with the standard Spalart-Allmaras turbulence model. For the laminar separated case, in which the oncoming boundary layer ahead of the separation point is laminar, the wakes are much wider and are accompanied by stronger shedding and modulations in flow quantities. For this case, the 2-D URANS solutions are found to be unreliable and erroneous. The 3-D URANS solutions show significant improvement compared with their 2-D counterpart, but are still too diffusive. When the TLNS3D code is run in the 3-D DES mode, the computed pressures agree well with the experimental data and previously published higher order 3-D DES solutions. In addition, the flow structure and time histories obtained with TLNS3D are very similar to these higher order solutions.

Based on this work, it appears that nominally second-order accurate, production type CFD codes such as TLNS3D could be used for predicting time-averaged properties for highly separated, unsteady flows, such as the ones encountered on a circular cylinder when run in the DES mode. However, care should be taken to ensure that appropriate grid resolution and time steps are chosen for such work. As expected, finer flow structures captured by the higher order schemes could not be reproduced accurately by a second-order scheme on comparable grids. Nonetheless, the resulting time-averaged pressure distributions can be predicted reliably and accurately with such schemes, thus establishing their applicability for computing average aerodynamic forces. One should be cautious about the use of such codes for applications in which the finer spatial and temporal structures affect the quantities of interest, such as aero-acoustic predictions, without further detailed analysis of the resulting solutions.

Acknowledgements

The authors would like to express their sincere gratitude to Drs. P. R. Spalart and M. Strelets for discussions regarding the cylinder test case and for sharing computational and experimental data.

References

- ¹Spalart, P.R., "Trends in turbulence treatments," AIAA Paper 2000-2306 (2000).
- ²Spalart, P.R., "Strategies for turbulence modeling and simulations," *Int. J. Heat Fluid Flow* vol. 21, 2000, pp. 252-263.

³Spalart, P.R., "Young Person's Guide to Detached-Eddy Simulation Grids," NASA CR-2001, 211032 (2001).

⁴Shur, M.L., Spalart, P.R., Strelets, M., and Travin, A., "Detached-Eddy simulation of an airfoil at high angle of attack," presented at the 4th International Symp. on Engineering, Turbulence Modeling and Measurements, Corsica, France, May 24–26, 1999.

⁵Spalart, P.R., Jou, W.H., Strelets, M., and Allmaras, S.R., "Comments on the feasibility of LES for wings, and on a hybrid RANS/LES approach," 1st AFOSR Int. Conf. on DNS/LES, Aug. 4–8, 1997. Ruston, LA, In "Advances in DNS/LES", C. Liu and Z. Liu Eds., Greden Press, Columbus, OH.

⁶Arunajatesan, S. and Sinha, N., "Unified Unsteady RANS-LES Simulations of Cavity Flowfields," AIAA Paper 2001-0516, Jan. 2001.

⁷Batten, P., Goldberg, U., and Chakravarthy, S., "LNS - An Approach Towards Embedded LES," AIAA Paper 2002-0427, Jan. 2002.

⁸von Terzi, D.A. and Fasel, H.F., "A New Flow Simulation Methodology Applied to the Turbulent Backward-Facing Step," AIAA Paper 2002-0429, Jan. 2002.

⁹Speziale, C.G., "Turbulence Modeling for Time-Dependent RANS and VLES: A Review," AIAA J., vol. 36, no. 2, Feb. 1998, pp. 173–184.

¹⁰Constantinescu, G.S., Pacheco, R., and Squires, K.D., "Detached-Eddy Simulation of Flow over a Sphere," AIAA Paper 2002-0425, Jan. 2002.

¹¹Forsythe, J.R., Hoffmann, K.A., and Squires, K.D., "Detached-Eddy Simulation with Compressibility Corrections Applied to a Supersonic Axisymmetric Base Flow," AIAA Paper 2002-0586, Jan. 2002.

¹²Forsythe, J.R., Squires, K.D., Wurtzler, K.E., and Spalart, P.R., "Detached-Eddy Simulation of Fighter Aircraft at High Alpha," AIAA Paper 2002-0591, Jan. 2002.

¹³Forsythe, J.R. and Hoffmann, K.A., "Detached-Eddy Simulation of a Supersonic Axisymmetric Base Flow with an Unstructured Solver," AIAA Paper 2000-2410, June 2000.

¹⁴Squires, K.D., Strang, W.Z., Wurtzler, K.E., Tomaro, R.E., Grismer, M.J., and Spalart, P.R., "Progress on Detached-Eddy Simulation of Massively Separated Flows," AIAA Paper 2002-1021, Jan. 2002.

¹⁵Spalart, P.R. and Allmaras, S.R., "A one-equation turbulence model for aerodynamic flows," *La Rech. Aerospaciale*, vol. 1, 1994, pp. 5–21.

¹⁶Menter, F.R., "Two-Equation Eddy-Viscosity Turbulence Models for Aerodynamic Flows," AIAA Paper 93-2906, 1993.

¹⁷Jameson, A., Schmidt, W., and Turkel, E., "Numerical Solutions of the Euler Equations by a Finite Volume Method Using Runge-Kutta Time-Stepping Schemes," AIAA Paper 81-1259, 1981.

¹⁸Jameson, A., "Time Dependent Calculations Using Multigrid, with Applications to Unsteady Flows past Airfoils and Wings," AIAA Paper 91-1596, 1991.

¹⁹Melson, N.D. and Sanetrik, M.D., "Multigrid Acceleration of Time-Accurate Navier-Stokes Calculations," 7th Cooper Mountain Conference on Multigrid Methods, 1995.

²⁰Bijl, H., Carpenter, M.H., and Vatsa, V.N., "Time Integration Schemes for the Unsteady Navier-Stokes Equations," AIAA Paper 2001-2612, June 2001.

²¹Travin, A., Shur, M.L., Strelets, M., and Spalart, P.R., "Detached-Eddy Simulations Past a Circular Cylinder," *Flow, Turbulence, and Combustion*, vol. 63, 2000, pp. 193–313.

²²Shur, M.L., Spalart, P.R., Strelets, M., and Travin, A., "Navier-Stokes simulations of shedding turbulent flow past a circular cylinder and a cylinder with a backward splitter plate." Appeared in: Third EC-COMAS CFD Conference, Paris, Sept. 1996, Desideri, G.A., Hirsh, C., Le Tallec, P., Pandolfi, M. and Periaux, J. (eds), John Wiley and sons, Chichester (1996) pp. 676–682.

²³Roshko, A., "Experiments on the flow past a circular cylinder at a very high Reynolds number," *J. Fluid Mech.*, vol. 10, no. 3, 1961, pp. 345–356.

²⁴van Nunen, J.W.G., "Pressure and forces on a circular cylinder in a cross flow at high Reynolds number." *Flow Induced Structural Vibrations*, Naudascher, E (ed.), Springer-Verlag, Berlin, 1974, pp. 748–754.

²⁵Cantwell, B., and Coles, D., "An experimental study of entrainment and transport in the turbulent near wake of a circular cylinder," *J. Fluid Mech.*, vol. 136, 1983, pp. 321–374.

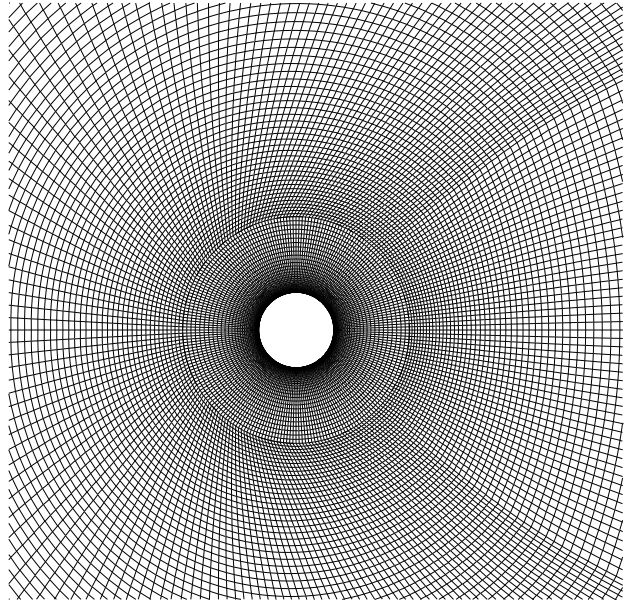


Fig. 1 Partial view of computational grid for circular cylinder

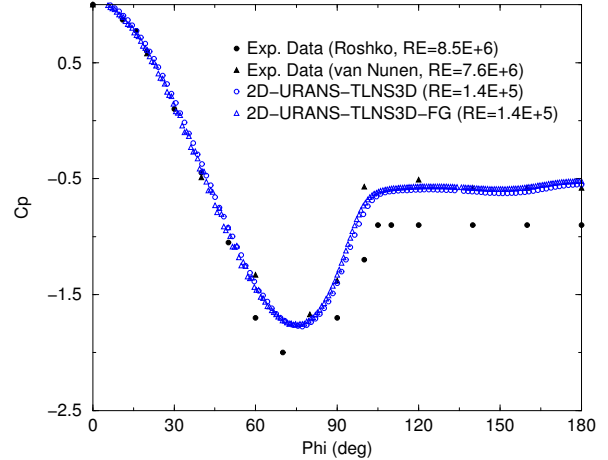


Fig. 2 Effect of grid refinement on pressure distribution for TS circular cylinder, 2D-URANS

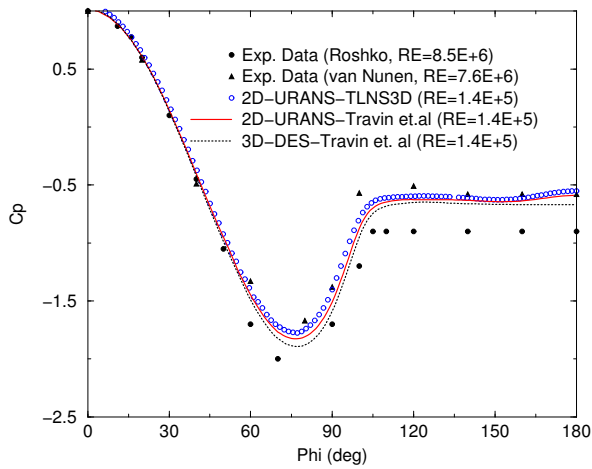


Fig. 3 Pressure distributions for TS circular cylinder

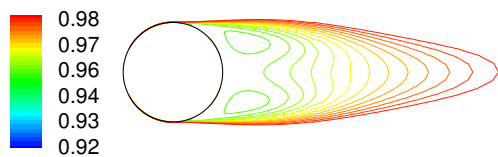


Fig. 4 Total Pressure contours for TS circular cylinder

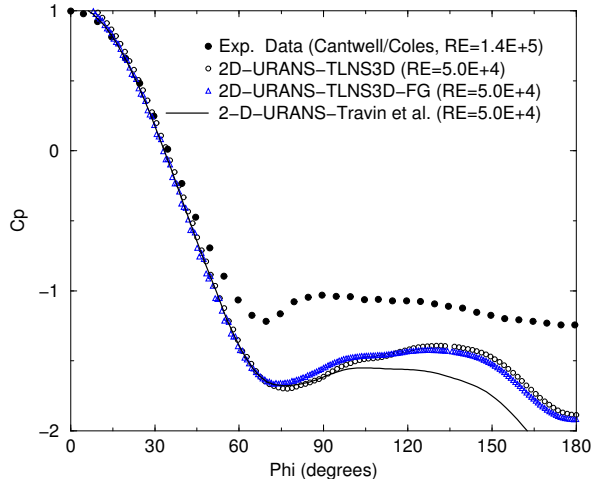


Fig. 5 Pressure distributions for LS circular cylinder, 2D-URANS

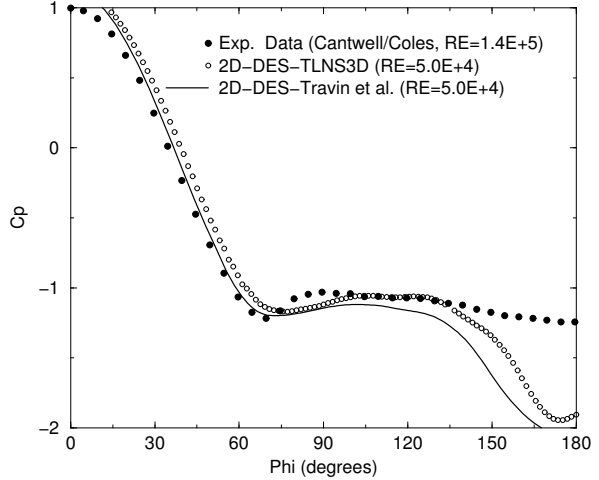


Fig. 6 Pressure distributions for LS circular, cylinder, 2D-DES

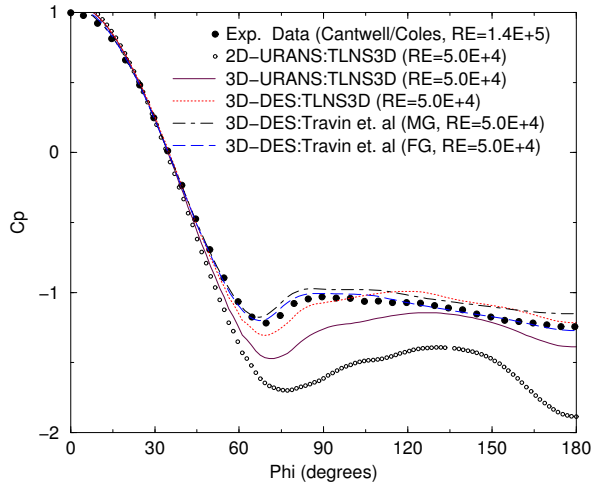


Fig. 7 Pressure distributions for LS circular cylinder for different schemes

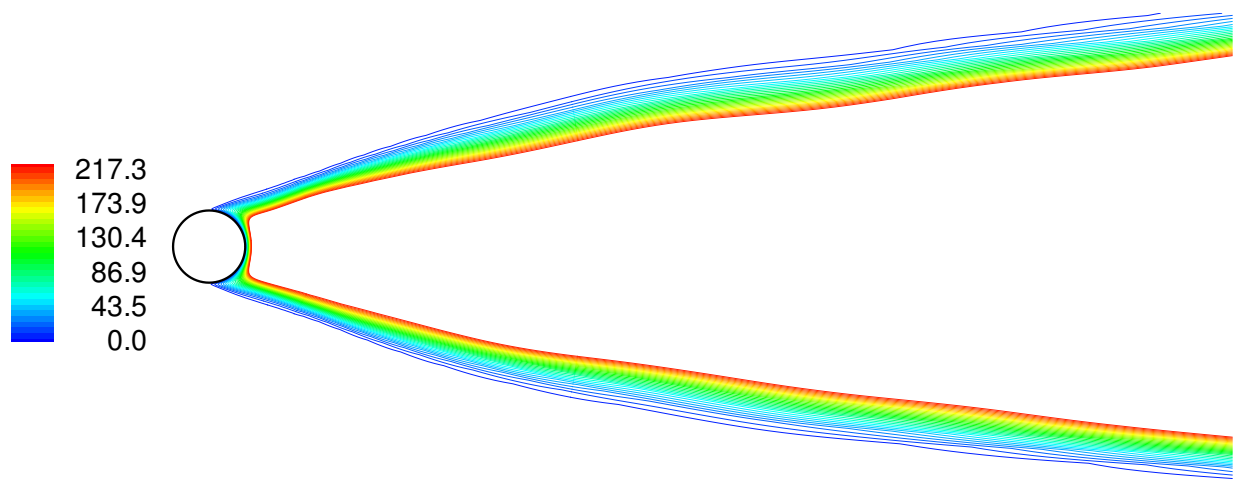


Fig. 8 Eddy viscosity contours for LS circular cylinder, 3D-URANS

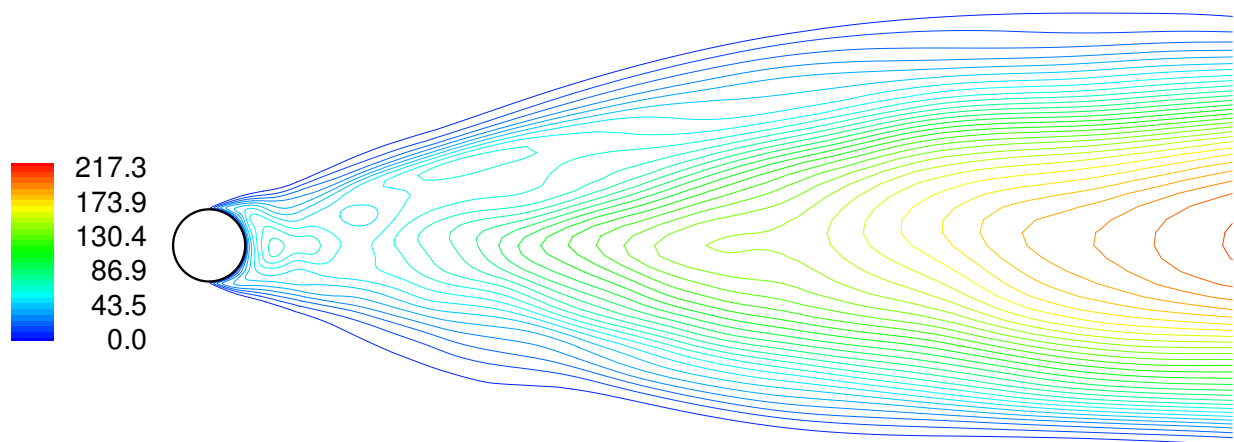


Fig. 9 Eddy viscosity contours for LS circular cylinder, 3D-DES

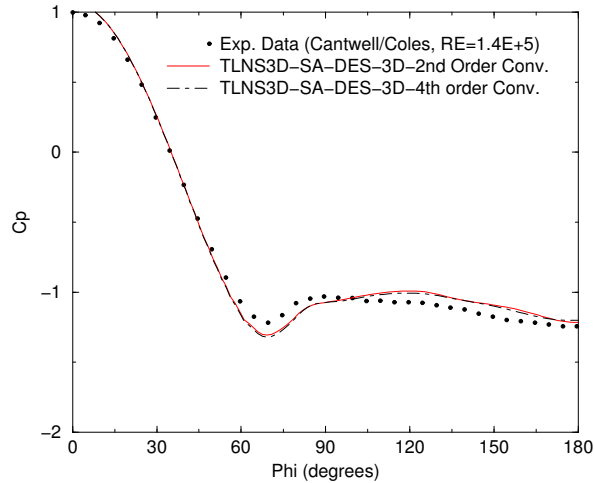


Fig. 10 Effect of higher order discretization for LS circular cylinder pressure distributions

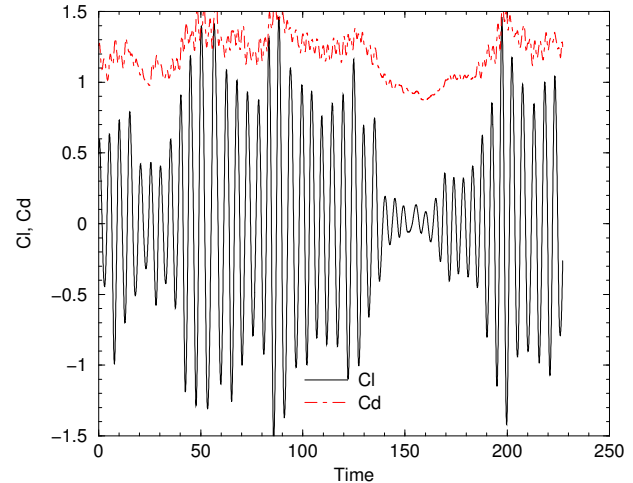


Fig. 12 Time history of integrated forces for LS circular cylinder, 3D-DES, 2nd order convection

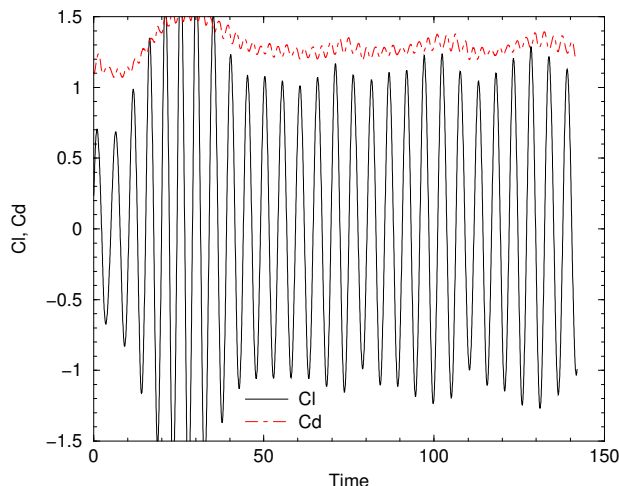


Fig. 11 Time history of integrated forces for LS circular cylinder, 3D-URANS

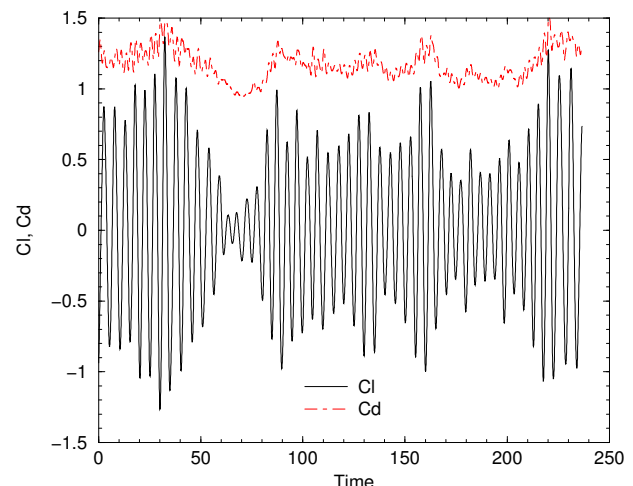


Fig. 13 Time history of integrated forces for LS circular cylinder, 3D-DES, 4th order convection

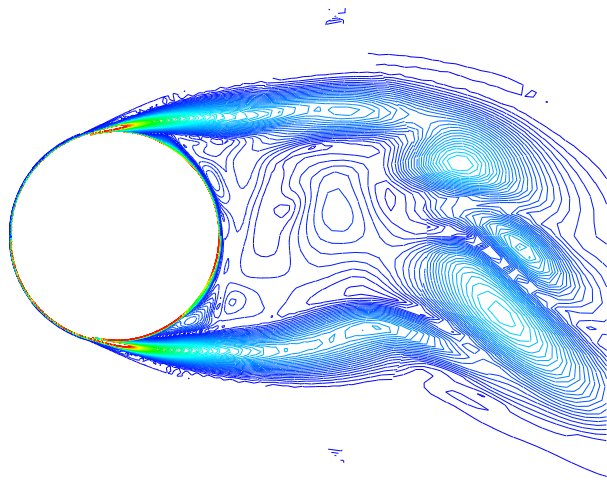


Fig. 14 Instantaneous vorticity contours for LS circular cylinder, 2nd order convection - near low lift-oscillations

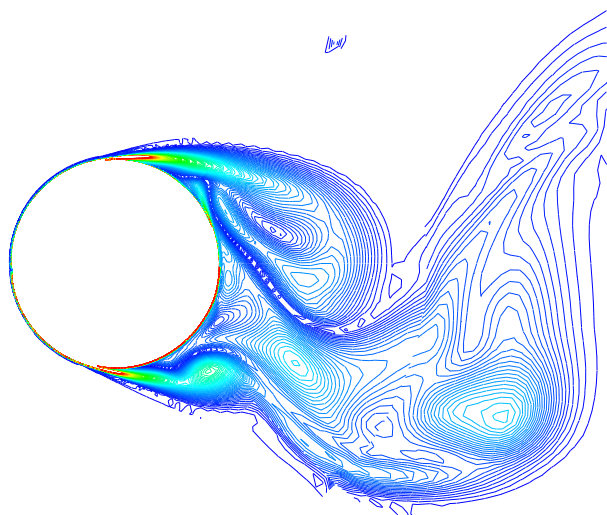


Fig. 15 Instantaneous vorticity contours for LS circular cylinder, 2nd order convection - near high lift-oscillations

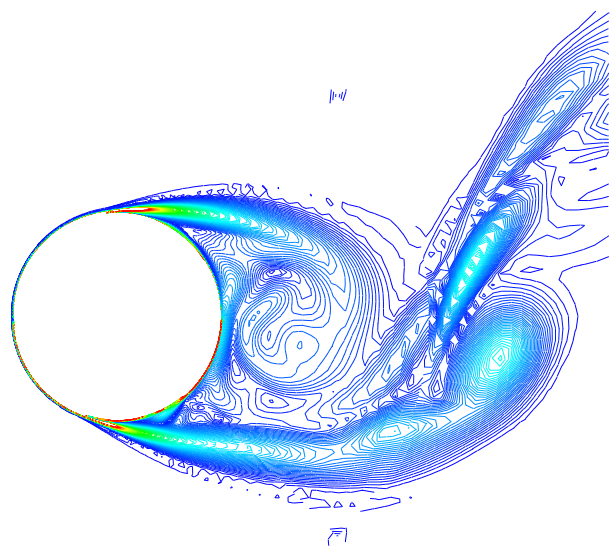


Fig. 16 Instantaneous vorticity contours for LS circular cylinder, 4th order convection - near high lift-oscillations